Clim. Past Discuss., doi:10.5194/cp-2015-170, 2016
Manuscript under review for journal Clim. Past
Published: 15 January 2016

Climate of the Past Discussions
Open Access

Dynamical downscaling of the western North Pacific from CCSM4 simulations during the last glacial maximum and late 20th century using the WRF model: model configuration and validation

J. Yoo and J. Galewsky

University of New Mexico, 221 Yale Blvd. NE MSC03 2040, Albuquerque, NM 87131-0001, USA

Received: 11 November 2015 – Accepted: 9 December 2015 – Published: 15 January 2016

Correspondence to: J. Yoo (jinwoong.yoo@gmail.com)

Published by Copernicus Publications on behalf of the European Geosciences Union.

Abstract

Using the Weather Research and Forecasting (WRF) model (version 3.5.1), dynamical downscaling of the Community Climate System Model, version 4 (CCSM4), simulations of the last glacial maximum (LGM) and 20th century (ensemble member #6) run were conducted to simulate ten years of climate over the western North Pacific during the LGM and modern climates, respectively. This paper describes the downscaling procedures for the Weather Research and Forecasting (WRF) model experiments and the quantitative and qualitative model validations comparing with the CCSM4 LGM and 20th century simulations results.

Results of the dynamical downscaling of the CCSM4 LGM paleoclimate and twentieth century using the WRF model show not only that the WRF model is capable of long-term simulations in the paleoclimate state of LGM, but also that the WRF model can correct biases in the general circulation model (GCM), producing more realistic spatial distributions of the pressure-level variables. The downscaling of a GCM model using the WRF model (36 km) for the regional climate simulation is considered computationally cost-effective and reliable from the perspectives of model thermodynamics in general, although there are some model errors still existing with dynamic variables.

1 Introduction

Over the past 21 000 years, the Earth has undergone a substantial warming induced by natural vacillations in orbital geometry, a concomitant rebound in greenhouse gas levels, and changing boundary conditions (i.e., ice sheet retreat and rising sea level). At the height of the last glacial maximum (LGM) 21 000 years ago (21 ka), the drop in CO_2 levels to 185 ppm, the drop in CH_4 to 350 ppb, and the far greater extent of ice coverage at high latitudes, are the most important forcing changes for the climate of the LGM, while seasonal and latitudinal distribution of incoming solar radiation at the top of Earth's atmosphere was the second largest difference from those of today (e.g.

Otto-Bliesner et al., 2006). Thus, surface temperatures in the LGM were about 2 °C lower in the tropics (Broccoli, 2000) and about 30 °C colder over the Laurentide ice sheet (Braconnot et al., 2007).

Downscaling of the paleoclimate can provide insights about the paleoclimate conditions that cannot be obtained otherwise by just compiling the proxy records. For example, horizontal and vertical spatial distributions of variables of interest can be inferred or conjectured realistically through the downscale modeling considering the large-scale climate condition as well as the proxy information. Geological studies have speculated about what synoptic scale patterns might have changed in the tropics, but global model simulations of paleoclimates offer synthetic data to compare with results from geologic proxies (Galewsky et al., 2006). Therefore, downscaling of general circulation model (GCM) output can provide a quantitative foundation for paleoenvironment research in a variety of applications.

The goal of this study is to downscale of the Community Climate System Model (version 4; CCSM4) LGM paleoclimate and twentieth century runs from the phase five of coupled model intercomparison project (CMIP5) and paleoclimate model intercomparison project version 3 (PMIP3) to understand the behavior of large-scale dynamics and thermodynamics over the western North Pacific under the LGM and present eras using the Weather Research and Forecasting (WRF) model. Specifically, the purpose of this paper is to address the following: (1) procedures to conduct a dynamical downscaling of the CCSM4 model outputs for the LGM and late modern simulations; and (2) evaluation of the downscaling performance of the WRF model by comparing the downscaling results with the GCM LGM paleoclimate and twentieth century simulation results.

This paper is organized as follows. In Sect. 2, we describe the preparation methods and procedures for the WRF model simulation set-up, specifically, for the LGM period. We discuss the validation of downscaling experiment results in Sect. 3. A discussion will follow in Sect. 4. A summary and conclusion are addressed in Sect. 5.

CPD
doi:10.5194/cp-2015-170

2 Data and methods

2.1 Domain configuration and model physics scheme

For the dynamical downscaling of the CCSM4, the Advanced Research WRF (ARW) model version 3.1.5 (Skamarock et al., 2005) was used. The WRF model has been shown capable of long-term climate simulations (e.g. Done et al., 2006; Yu et al., 2014). The WRF model in this study employs a terrain following non-hydrostatic pressure vertical coordinate with 51 levels and the model top at 10 hPa. We set our model domain over the western North Pacific both for the LGM and the modern (Fig. 1). Each computational grid has a 36 km horizontal resolution with 171 latitude points by 282 longitude points. The WRF model domain latitudes range from 13.066° S to 47.435° N and the domain longitude range from 93.75° E to 206.25° E. The adaptive time step option was applied for the actual integrations with an average time step (dt) of about 74 s. Except for the modified community atmosphere model (CAM) shortwave and longwave radiation schemes for the LGM climate simulation, model physics and dynamic schemes employed for the LGM and the modern simulations are identical. The ARW (version 3) modeling system user's guide (National Center for Atmospheric Research (NCAR), 2014) was referenced to configure the model physics schemes: WRF Single-Moment 6-class scheme for microphysics; CAM scheme for shortwave and longwave radiation schemes; the Pennsylvania State University/NCAR mesoscale model version 5 (MM5) similarity scheme based on Monin–Obukhov with Carslon–Boland viscous sub-layer for surface layer option; Noah Land Surface Model represents surface processes; Yonsei University planetary boundary layer (PBL) scheme represents boundary layer; Cumulus convection is parameterized with the Kain–Fritsch (new Eta) scheme; model sea surface temperature (SST) and skin temperature are updated every time step. CAM radiation scheme for the LGM simulation was modified to be consistent with the LGM radiation of the PMIP3/CMIP5 experiment accounting for the different forcing that are related with atmospheric concentration ratios of CO_2, CH_4, NO_2 and Earth's orbital parameters (i.e., eccentricity, obliquity, and angular presession of the Earth) as recommended by the PMIP2 project (Braconnot et al., 2007; Table 1).

2.2 LGM topography, ice sheet, and CCSM4 data preprocessing

Brady et al. (2013) conducted the simulation of the 21 ka LGM climate using the CCSM4. The main purposes of simulating the LGM by the PMIP3 and the CMIP5 were trifold: (1) to evaluate the model response to ice-age boundary conditions relative to paleodata, (2) to provide empirical constraints on global climate sensitivity, (3) to constrain climate sensitivity using climate models with paleorecords (Brady et al., 2013 and others therein). The CCSM4 is a GCM consisted of four major components for the atmosphere (Community Atmosphere Model version 4 (CAM4); Neale et al., 2013), ocean (NCAR implementation of the Parallel Ocean Program version 2 (POP2); http://www.cesm.ucar.edu/models/ccsm4.0/pop/; Brady et al., 2013), land (Community Land Model version 4 (CLM4); Lawrence et al., 2012), and sea ice (Briegleb et al., 2004). Those components are combined through a coupler (Gent et al., 2011). For more detail on the CCSM4 model configuration, see Brady et al., 2013.

Discernable differences in the LGM topography are the exposed land due to the globally retreated shore line (e.g. Southeast Asia) and the continental ice sheets in the North America and the Northern Europe. The North American ice sheet region of the PMIP3/CMIP5 LGM ice sheet topography, which is included in the LGM CCSM4 forcing files, was blended with the one degree grid resolution topography of PMIP2 ICE-5G (v. 1.2) (Peltier, 2004) to represent the LGM topography and continental ice sheets correctly in the WRF model downscaling simulation with 36 km grid space resolution. The PMIP3/CMIP5 LGM ice sheets are also a blended average product among three different ice sheet reconstructions (Brady et al., 2013): ICE-6G v2.0 (Argus and Peltier, 2010), Meltwater routing and Ocean–Cryosphere–Atmosphere response (MOCA; Tarasov and Peltier, 2004), and Australian National University (ANU; Lambeck et al., 2010). The ice sheet mask of the ICE-5G data was used to delineate the ice sheet boundary over the blended LGM topography to assign the soil property appropriately in the WRF model boundary as ice-covered (Fig. 1). Although our western North Pacific domain did not need the ice sheet, it is essential for North American or tropical channel simulations.

Since the CCSM4 LGM simulation is part of the PMIP3/CMIP5 set of simulations, the vegetation in the simulation of this study should be treated as in the CMIP5 preindustrial (PI) experiment where model vegetation was prescribed to PI with interactive leaf area index (LAI) (models with interactive carbon cycle, but no vegetation dynamics) for CCSM4 (B. Otto-Bliesner, 2013, personal communication). Although, the vegetation phenology (LAI and canopy heights) differ between the LGM and PI simulations (B. Otto-Bliesner, 2013, personal communication). Therefore, the land use land cover (LULC) in the default WRF model with the 24-Category USGS land use category are retained except for the LGM ice sheet area and the exposed land area due to the retrieved shoreline for the LGM simulation. For the LULC over the exposed land surface, Climate Long-Range Investigation, Mapping, and Prediction (CLIMAP) LGM vegetation was remapped to USGS 24-category land use categories referencing the vegetation types in "Details of the vegetation scheme used for the map reconstructions" (http://www.esd.ornl.gov/projects/qen/adams3.html) (Table 2 and Fig. 1). Albedo and green fraction information over the ice sheet and the exposed land in the LGM were also generated from the forcing files of the PMIP3/CMIP5 LGM experiment for the usage in the WRF LGM simulation. For the modern simulation, default WRF topography and LULC data were implemented (Fig. 1).

2.3 Retrieving CCSM4 data

We obtained 6 hourly PMIP3/CMIP5 data in NetCDF format of both paleoclimate runs and the 20th century MOAR control simulation from the University Corporation for Atmospheric Research (UCAR) Yellowstone data storage (a.k.a. HPSS). The latter are also available at http://www.cesm.ucar.edu/experiments/cesm1.0/. The CCSM4 NetCDF file was converted into GRIB file for the WRF model input by using a community package called cam_to_wps (B. Fisel, 2014, personal communication; adopting

CPD
doi:10.5194/cp-2015-170

Dynamical downscaling of the western North Pacific from CCSM4 simulations

J. Yoo and J. Galewsky

Ruby Leung's Fortran program) with a slight modification to correct some critical errors existing in the code. The modification of the code also includes enhancing the vertical profiles of soil moisture and soil temperature in the four soil layers for the long-term climate simulation, eliminating the monotonicity in the soil properties in the vertical column by the community code. We used six hourly pressure level data of the CCSM4 as WRF input data for 3-dimensional pressure levels (e.g. pressure, temperature, zonal/meridional winds, and geopotential), and 2-dimensional surface such as 2 m air temperature ($T2$), 2 m relative humidity (RH2), and 10 m winds ($U10$ and $V10$). We also used daily outputs of CCSM4 data for sea surface temperature (SST), sea ice content, top layer soil water (SOILWATER_10CM), and top layer soil temperature (TSOI_10CM). The vertical profiles of soil moisture and soil temperature were created by blending the CCSM4 daily data of top layer soil values with the CLM4 monthly mean of soil vertical profiles at three different soil depths at 0.25, 0.7, and 1.5 m. Total model integrations periods of the LGM and the modern simulations are ten years each from PMIP3/CMIP5 model simulation years from 1871 to 1880 and from 1990 to 1999, respectively. Since Year 1870 was the initialization year of the PMIP3/CMIP5 paleoclimate LGM simulation, we chose Year 1871 to be the first year of the LGM simulation to avoid any issue associated with the CCSM4 model spin-up. WRF model simulations were re-initialized every year on 1 January at 00:00 UTC.

3 Validation of model results

In part due to the lack of observational data during the LGM period for direct comparisons and in part due to the fact that our downscaling simulations are part of long-term simulations, model validations are conducted by evaluating the WRF forecast skills against the PMIP3/CMIP5 CCSM4 simulation results as the "control". We adopt correlation coefficient (r) and root mean square error (RMSE) as statistical measurements.

CPD
doi:10.5194/cp-2015-170

RMSE is one of the commonly used error statistics defined as

$$\mathrm{RMSE} = \sqrt{\frac{1}{N}\sum_{i=1}^{N}(M_i - O_i)^2}, \tag{1}$$

where N is the total number of grid points and M and O represent the values of variables from WRF and CCSM4 simulations, respectively. The difference of domain average from the WRF and CCSM4 results was also computed. To facilitate comparisons between two different model grid resolutions, the WRF results (36 km; 171 × 282) were regridded horizontally into that of CCSM4 grids (1.25° latitude × 0.9° longitude; 66 × 91) using the Earth System Modeling Framework (ESMF) software.

3.1 Incoming solar radiation

Incoming solar radiation at the top of the model atmosphere is the fundamental source of energy driving the cascade of energy flow in the climate model. Incoming solar radiation at the top of the atmosphere does not change significantly annually but it is solely dependent on the radiation physics implemented in each model. Figure 2 shows 10 year averages of the latitudinal and temporal distributions of incoming solar radiation at the top of atmosphere (TOA) both in the CCSM4 (top) and the downscaled WRF model (bottom). Left, center, and right panels represent LGM, modern, and the difference between the two periods, respectively. The comparison between the two difference plots shows that the modified CAM radiation schemes for the downscaling experiments using the WRF model reproduced the characteristics of the spatio-temporal solar radiation distribution present in the CCSM4 LGM simulation outputs. Their comparability between the CCSM4 and the WRF results suggests the validity of the modified CAM radiation schemes for the downscaling experiments using the WRF model.

CPD
doi:10.5194/cp-2015-170

3.2 2 m air temperature

Figure 3 shows comparison of ten year averages of 2 m air temperature ($T2$) both from WRF and CCSM4 simulations for LGM and late modern periods. Ten-year domain average (standard deviation, SD) of $T2$ from the LGM WRF simulation was 16.08 (10.07) °C, while that from the CCSM4 LGM simulation was 18.05 (9.17) °C. WRF bias (WRF-CCSM4) for the LGM simulations was −1.04 (1.45) °C and RMSE was 1.78 (Fig. 3). Correlation coefficient (r) between the two long-term averages was 0.99. On the other hand, ten year domain average (SD) of $T2$ from the Modern WRF simulation was 20.37 (8.42) °C, while that from the CCSM4 modern simulation was 22.07 (7.68) °C. WRF bias (WRF-CCSM4) for the modern WRF simulations was −0.95 (1.34) °C and RMSE was 1.64. r between the two long-term averages was also 0.99 for the Modern simulations (Fig. 3).

$T2$ difference map between the LGM and Modern from the WRF downscaling simulations (Fig. 3 upper-right plot) resembles closely that from the CCSM4 simulations (Fig. 3 middle-right plot). The average of the difference between the two plots was −0.09 °C and r between the two was 0.93 (Fig. 3 lower-right). This suggests that the WRF model simulations reproduced the cold LGM climate correctly geographically. Note that decrease of boundary layer temperature during the LGM is greater in the high latitudes than in the lower latitudes, which is consistent with literature (Broccoli, 2000; Braconnot et al., 2007; Korty et al., 2012). Comparisons of $T2$ between the WRF and CCSM4 simulations during both the LGM (left column) and late modern (center column) show that the WRF model produced negative biases slightly overall. It seems that those negative biases are spatially clustered over the midlatitude coastal region and its downwind region. Considering only for the LGM simulation results, ten year average (SD) of $T2$ over the land only from the WRF simulation was 8.62 (11.01) °C, while that from the CCSM4 was 11.81 (10.97) °C. WRF bias (WRF-CCSM4) was −0.90 (1.65) °C and RMSE was 1.88 (not shown). Apparently, $T2$ over the land was colder than over the ocean and $T2$ over the land has more variability (with higher SD) than when the

CPD
doi:10.5194/cp-2015-170

ocean combined. However, the WRF bias was slightly reduced with $T2$ over the land only.

On the other hand, latitudinal and monthly distributions of ten year averages of $T2$ from the WRF and CCSM4 simulations both for the LGM and modern periods (Fig. 4) suggest also that the WRF downscaling simulations reproduced the temporal variance of $T2$ in the CCSM4 results well in general. It is notable, however, that compared to the CCSM4 simulations, the WRF simulations underpredicted $T2$ during the summer season and overpredicted $T2$ during the fall and winter seasons over the region poleward of 15° N, while they slightly overpredicted $T2$ over tropical region (13° S–10° N) from March to December. The tendency of underprediction of $T2$ was stronger in the modern simulation than in the LGM simulation. These deviations from the CCSM4 results may be attributable in part to the model physics (Lo et al., 2008) and the higher spatial resolution in the WRF simulations. Model bias can be introduced also from calculating the zonal averages and regridding the relatively higher resolution of WRF results to match with the coarse CCSM4 grids.

Considering only land values, 10 year monthly climate of $T2$ shows that the WRF simulation under-predicted the $T2$ through the year (Fig. 5). But the model bias remained within the magnitude of 1.3 °C (-1.3 °C $\leq$ bias $\leq$ -0.29 °C). SD of $T2$ has a strong seasonality with high in summer and low in winter in both the WRF and CCSM4 simulations. However, WRF model bias and SD of the bias did not vary much through the season. It is also notable that some of model biases are attributable to the regridding of WRF result, which is unavoidable in the model comparison.

To evaluate the WRF forecast error with the time varying $T2$ further in detail, we compared the time series of domain averages of $T2$ between the WRF and CCSM4. To keep data processing at manageable levels, a sampling method was used here. That is, out of 14 600 time stamps of the whole 10 year six-hourly model simulation results for the WRF and the CCSM4 each, weekly data (total of 522 samples) were collected and compared from the initial time of the simulations. All the time stamps of the sampled model results should be 00:00 UTC.

CPD
doi:10.5194/cp-2015-170

Over the entire model domain, $T2$ average of the sampled CCSM4 LGM simulation results was 17.03 °C, while that of the WRF simulation was 15.62 °C. Also, the mean of the WRF forecast error (bias: WRF – CCSM4) was −0.46 °C, and the average of RMSE was 2.17 (Fig. 6, Table 3). The counterparts in the modern simulations were 22.02, 19.98, −1.25, and 3.09 °C for the CCSM4, WRF model simulations, model forecast error, and the RMSE, respectively (not shown). Note that the WRF model bias and RMSE in the LGM are less than those of modern. It is clearly notable that the downscaled WRF LGM simulation result was about 4 °C colder than that of the modern simulation, which is consistent with one of the defining characteristics of the LGM (Brady et al., 2013). Table 3 summarizes WRF model performance with average, (normalized) forecast errors, and RMSE from the time series of major variables over the ten year simulation period. Variables include $T2$, soil moisture at 5 cm depth (SMOIS), soil temperature at 5 cm depth (TSLB), RH2, 10 m U wind ($U10$), 10 m V wind ($V10$), sea level pressure (SLP), geopothential height (GHT), 850 hPa temperature (TT), 850 hPa U-wind (UU), and 850 hPa V-wind (VV). It is notable that WRF model forecast errors were relatively small in general but wind component variables at 10 m height and 850 hPa level have relatively high errors both in the LGM and Modern simulations.

3.3 2 m relative humidity and total precipitable water

Along with $T2$, atmospheric moisture in the near surface and in the vertical column is a critical component in the model thermodynamics. To evaluate the downscaling performance in this feature, relative humidity at 2 m (RH2) and total precipitable water (TPW) are examined in this section.

Ten years domain average (SD) of RH2 from the WRF LGM simulation was 85.88 (9.8) %, while that from the CCSM4 was 79.14 (5.96) %. Average WRF bias for the LGM simulations was 6.41 (7.98) % and the RMSE was 10.22. Correlation coefficient of RH2 between the WRF and the CCSM4 simulation averages was 0.51 (Fig. 7). Likewise, ten years domain average (SD) of RH2 from the WRF Modern simulation was 87.5 (7.71) %, while that from the CCSM4 Modern simulation was 79.91 (4.13) %. Av-

CPD
doi:10.5194/cp-2015-170

erage WRF bias for the Modern simulations was 7.39 (6.57) % and the RMSE was 9.89. Correlation coefficient of RH2 between the WRF and the CCSM4 Modern simulation averages was 0.42 (Fig. 7). Comparisons of the mean RH2 between the WRF and the CCSM4 simulations suggests that (1) the WRF model produced wet biases both in the LGM and the Modern simulations in general, (2) in both the LGM and the Modern simulations, the WRF model produced dry biases over the land in general while producing strong wet biases over Tibet Plateau and Korea/Japan regions.

Spatial distributions of RH2 differences between the LGM and the Modern simulations resemble each other for the WRF and the CCSM4 simulations in general. The WRF downscaling simulations reproduced well the drier continental surface during the LGM than that in the Modern climate. It is notable that RH2 over the open ocean does not differ between the LGM and the Modern both for the WRF and the CCSM4 simulations but the WRF simulations produced relatively strong dry biases compared to CCSM4 over the exposed land area at the LGM, in particular, near the Maritime continent. It seems that differences in model physics and in land surface model that are implemented in the WRF downscaling simulations are attributable to those spatial difference of RH2.

Considering LGM RH2 over land values only, monthly climate of RH2 shows that the downscaled WRF simulation underpredicted RH2 about 10 % yearly compared to the CCSM4 (Fig. 8). The WRF model bias contains a weak seasonal cycle ranging from −11.01 % in December to −2.7 % in August which is coupled with its RSME. Interestingly, both the WRF and CCSM4 simulations have two months of RH2 minima in April (WRF: 65.11 % and CCSM4: 74.74 %) and October (67.99 and 74.13 %). Latitudinal and monthly distributions of ten year averages of RH2 (Fig. 9) also suggest that compared to the CCSM4 results, the WRF simulations produced relatively strong wet biases over 10 ~ 30° N latitudes. It seems that the wet biases over the ocean in the WRF simulations are mostly attributable to these positive biases in the zonal mean in both the LGM and Modern simulations (see Fig. 7). This tendency seems to be also associated with $T2$ distributions (see Fig. 4).

Discussion Paper | Discussion Paper | Discussion Paper | Discussion Paper |

CPD

doi:10.5194/cp-2015-170

Dynamical downscaling of the western North Pacific from CCSM4 simulations

J. Yoo and J. Galewsky

Meanwhile, ten years domain average (SD) of TPW from the WRF LGM simulation was 26.68 (12.08) mm vs. 29.55 (11.44) mm from the CCSM4 simulation (Fig. 10). Domain average WRF model bias (SD) and the RMSE for the LGM simulations were −1.79 (2.80) mm and 3.33, respectively. r between TPWs from the WRF LGM and the CCSM4 LGM simulations was 0.97. On the other hand, ten years domain average (SD) of TPW from the WRF Modern simulation was 35.39 (14.55) mm vs. 38.13 (13.14) mm from the CCSM4 Modern simulation. Domain average WRF bias and the RMSE in TPW for the Modern simulations were −1.42 (3.36) mm and 3.65, respectively. r of TPW between the WRF and the CCSM4 simulations was 0.97 in the modern case. Thus, WRF model both in LGM and Modern simulations reproduced TPWs of the CCSM4 results relatively well ($r = 0.97$). Still, the WRF has a tendency to overpredict TPWs over the western tropical Pacific and to underpredict over the southeastern China Sea while the spatial distributions of TPWs resemble each other between the WRF and the CCSM4 simulations (Fig. 10).

3.4 Vertical distribution of 3-dimensional variables

Examining vertical distribution of key dynamic and thermodynamic variables of three-dimension is useful and necessary to evaluate the performance of the downscaling model simulations. Figure 11 shows vertical plots of the ten years zonal averages of atmospheric temperature (T) and relative humidity (RH) comparing CCSM4 and WRF results from their LGM simulations. The WRF LGM simulation reproduced the vertical distribution of T in the CCSM4 LGM simulation closely. RH plot from the WRF LGM simulation resembles that from the CCSM4 LGM simulation except in the tropical upper-level atmosphere. It seems that relatively high RH in the tropical upper-level atmosphere in the CCSM4 results are model bias in the CCSM4 LGM simulation. However, the WRF simulation seems to have corrected the moist bias in the tropical upper-level RH in the CCSM4, producing reasonable relative humidity in vertical as well as in latitudes. The same plot but for the Modern simulations shows the similar bias in the CCSM4 simulation and the corrected vertical distributions of RH in the WRF simula-

CPD
doi:10.5194/cp-2015-170

tion (not shown). It is notable that the WRF downscaling simulations reproduced the vertical and latitudinal characteristics of relative humidity reasonably well (Fig. 11d): relatively high RH in the tropical latitudes and relatively low RH in the mid-latitude at the midtroposphere, resembling the Hadley circulation.

Figure 12 presents the comparisons between the CCSM4 and WRF results from their LGM simulations with the ten years climatology of zonal averages of zonal wind (U) and meridional wind (V). Apparently, both the U and V from the CCSM4 LGM simulation were reproduced comparably in the WRF LGM simulation. The WRF downscaling experiment has closely simulated tropical easterly winds and midlatitde westerly winds balancing each other over the extratropical latitudes (10–30° N) over the model domain.

Note that lower-level easterly winds were slightly enhanced in the WRF simulations over the CCSM4 simulations. The zonal averages of U from the WRF downscaled simulation clearly depicts the zone of enhanced easterly winds in the low-level atmosphere over the western North Pacific, which is one of the critical components of tropical cyclone development over the region, as well as the enhancement of westerly winds in the upper-level atmosphere in the midlatitude, which represents the midlatitude upper-level jet stream. On the other hand, the meridional wind (V) for the CCSM LGM simulation (Fig. 12c) shows the large-scale general circulation patterns with reduced magnitudes. In contrast, the zonal climatology of V from the WRF LGM downscaling simulation (Fig. 12d) clearly represents tropical convergence (divergence) in the low-level (upper-level) atmosphere which is the characteristic of Inter-Tropical Convergence Zone (ITCZ). Also depicted are the upper-level convergent flow over 20° N and the low-level divergence over 30° N. The same plots but for the Modern simulation show the similar vertical distributions of U and V in the CCSM4 and WRF simulations (not shown). Compared to the WRF LGM simulation, the WRF Modern simulation produced slightly enhanced magnitudes both in U and V in the Southern Hemisphere.

doi:10.5194/cp-2015-170

4 Discussion

Boundary or surface conditions play a critical role in the climate model simulations. In a long-term climate simulation of the modern climate, among the boundary variables updating SST once a day may be the most important input variable to check to avoid the model simulation drift from the long-term average. The other time-varying boundary inputs (such as vegetation, soil moisture/temperature, albedo, etc.) are controlled by climatology data, which do not vary much over time under the current climate. However, to simulate a different climate state like the LGM, modelers should be careful with their choice in constructing those time-varying boundary variables. While SST will be provided by the GCM, the other boundary variables should be determined and provided by the modeler. The more difficult choice should be made to determine the vegetation over the exposed land only during the LGM period due to the retrieved shorelines along the coast region in the Asia (Fig. 1). Since model simulation cannot be executed without the boundary conditions reconstructed for the LGM condition and those conditions cannot be modified during the execution, there is a clear limitation of long-term paleoclimate simulation, especially with the LGM. Paleoclimate reconstruction research with proxy records might reduce the uncertainty in the geographical extents of boundary input variables in the future.

5 Summary and conclusion

A study of a dynamical downscaling of the CCSM4 LGM paleoclimate and twentieth century runs from the CMIP5/PMIP3 was conducted using the WRF model in 36 km grid spatial resolution. The goal of the study is to investigate the behavior of large-scale dynamic and thermodynamic variables in the downscaling experiments over the western North Pacific under the LGM and modern climates. The model integrations periods of the LGM and the modern simulations were ten years from 1871 to 1880 and from 1990 to 1999, respectively.

CPD
doi:10.5194/cp-2015-170

In this paper, we described procedures to conduct a dynamical downscaling of the CCSM4 model outputs for the LGM and late modern simulations. In particular, to realize the LGM topography properly in the downscaling WRF model simulation, PMIP 2 ICE-5G data (v. 1.2) (Peltier, 2004) and PMIP3/CMIP5 LGM ice sheets data was used to modify the WRF geographic data (GEOG) to represent the LGM topography and continental ice sheets close to those of the CCSM4 LGM simulation.

For the model validation, the results from the WRF simulations were compared with the CCSM4 LGM paleoclimate and twentieth century simulation results using the ESMF regrid software for the quantitative and statistical comparison. Using 10 year averages of the forecast error (the difference between the WRF and CCSM4 simulations) for evaluated variable ($T2$, SMOIS, TSLB, RH2, $U10$, $V10$, SLP, GHT, TT, UU, and VV) (Table 3), it was shown that the WRF downscaling experiments reproduced the thermodynamic conditions closely to those of the CCSM4 LGM and Modern simulation results in general.

Overall, results of the dynamical downscaling of the CCSM4 LGM paleoclimate and twentieth century using the WRF model suggest that the WRF model is capable of long-term simulations in a different climate state in the past. Moreover, comparisons of vertical distributions of three-dimensional variables (T, RH, U, and V) suggest that the WRF model can correct biases in the GCM model, partly attributable to the low grid resolution, and produce more realistic spatial distribution patterns of the pressure-level variables, presumably, partly due to model physics and enhancement in the spatial resolution. It seems that the downscaling of a GCM model using the 36 km grid resolution WRF model for the regional climate simulation is computationally cost-effective and reliable from the perspectives of model thermodynamics in general while there are some forecast errors still existing with dynamic variables. This study might thus profitably contribute to dynamical downscaling studies of the paleoenvironment as well as regional climate change studies.

Acknowledgements. This work is supported by National Science Foundation (NSF)/Division of Atmospheric and Geospace Sciences (AGS) award 1064081 to J. Galewsky.

CPD
doi:10.5194/cp-2015-170

References

Argus, D. F. and Peltier, W. R.: Constraining models of postglacial rebound using space geodesy: a detailed assessment of model ICE-5G (VM2) and its relatives, Geophys. J. Int., 181, 697–723, 2010.

Braconnot, P., Otto-Bliesner, B., Harrison, S., Joussaume, S., Peterchmitt, J.-Y., Abe-Ouchi, A., Crucifix, M., Driesschaert, E., Fichefet, Th., Hewitt, C. D., Kageyama, M., Kitoh, A., Laîné, A., Loutre, M.-F., Marti, O., Merkel, U., Ramstein, G., Valdes, P., Weber, S. L., Yu, Y., and Zhao, Y.: Results of PMIP2 coupled simulations of the Mid-Holocene and Last Glacial Maximum – Part 1: experiments and large-scale features, Clim. Past, 3, 261–277, doi:10.5194/cp-3-261-2007, 2007.

Brady, E. C., Otto-Bliesner, B. L., Kay, J. E., and Rosenbloom, N.: Sensitivity to glacial forcing in the CCSM4, J. Climate, 26, 1901–1925, 2013.

Briegleb, B. P., Bitz, C. M., Hunke, E. C., Lipscomb, W. H., Holland, M. M., Schramm, J. L., and Moritz, R. E.: Scientific description of the sea ice component in the Community Climate System Model, Version 3, NCAR Tech. Note NCAR/TN-463+STR, 70 pp., NCAR, USA, 2004.

Broccoli, A. J.: Tropical cooling at the Last Glacial Maximum: an atmosphere–mixed layer ocean model simulation, J. Climate, 13, 951–976, 2000.

Done, J. M., Leung, L. R., and Kuo, Y.-H.: Understanding error in the long-term simulation of warm season rainfall using the WRF model, in: 7th WRF Users Workshop, Boulder, CO, USA (Extended Abstract), 2006/06/19, 2006.

Galewsy, J., Stark, C. P., Dadson, S., Wu, C.-C., Sobel, A. H., and Horng, M.-J.: Tropical cyclone triggering of sediment discharge in Taiwan, J. Geophys. Res., 111, F03014, doi:10.1029/2005JF000428, 2006.

Gent, P. R., and Gokhan, D., Donner, L. J., Holland, M. M., Hunke, E. C., Jayne, S. R., Lawrence, D. M., Neale, R. B., Rasch, P. J., Vertenstein M., Worley, P. H., Yang, Z.-L., and Zhang, M.: : The Community Climate System Model version 4, J. Climate, 24, 4973–4991, 2011.

Korty, R. L., Camargo, S. J., and Galewsky, J.: Tropical cyclone genesis factors in simulations of the last glacial maximum, J. Climate, 25, 4348–4365, 2012.

Lambeck, K., Purcell, A., Zhao, J., and Svensson, N.-O.: The Scandinavian ice sheet: from MIS 4 to the end of the last glacial maximum, Boreas, 39, 410–435, doi:10.1111/j.1502-3885.2010.00140.x, 2010.

CPD
doi:10.5194/cp-2015-170

Dynamical downscaling of the western North Pacific from CCSM4 simulations

J. Yoo and J. Galewsky

Lawrence, D. M., Oleson, K. W., Flanner, M. G., Fletcher, C. G., Lawrence, P. J., Levis, S., Swenson, S. C., and Bonan, G. B.: The CCSM4 land simulation, 1850–2005: assessment of surface climate and new capabilities, J. Climate, 25, 2240–2260, 2012.

Lo, J. C.-F., Yang, Z.-L., and Pielke Sr., R. A.: Assessment of three dynamical climate downscaling methods using the Weather Research and Forecasting (WRF) model, J. Geophys. Res., 113, D09112, doi:10.1029/2007JD009216, 2008.

NCAR: Weather Research & Forecasting ARW Version 3 Modeling System User's Guide, NCAR, USA, 2014.

Neale, R. B., Richter, J., Park, S., Lauritzen, P. H., Vavrus, S. J., Rasch, P. J., and Zhang, M. 2013: The mean climate of the Community Atmosphere Model (CAM4) in forced SST and fully coupled experiments, J. Climate, 26, 5150–5168, 2013.

Otto-Bliesner, B., Brady, E. C., Clauzet, G., Tomas, R., Levis, S., and Kothavala, Z.: Last glacial maximum and holocene climate in CCSM3, J. Climate, 19, 2526–2544, 2006.

Peltier, W. R.: Global glacial isostasy and the surface of the ice-age Earth: the ICE-5G(VM2) model and GRACE, Annu. Rev. Earth Pl. Sc., 32, 111–149, 2004.

Skamarock, W. C., Klemp, J. B., Dudhia, J., Gill, D. O., Barker, D. M., Wang, W., and Powers, J. G.: A description of the advanced research WRF Version 2, NCAR Technical Note TN-468 STR, NCAR, USA, 88 pp., 2005.

Tarasov, L. and Peltier, W. R.: A geophysically constrained large ensemble analysis of the deglacial history of the North American ice-sheet complex, Quaternary Sci. Rev., 23, 359–388, 2004.

Yu, E., Wang, T., Gao, Y., and Xiang, W.: Precipitation pattern of the mid-Holocene simulated by a high-resolution regional climate model, Adv. Atmos. Sci., 31, 962–971, doi:10.1007/s00376-013-3178-9, 2014.

CPD
doi:10.5194/cp-2015-170

Dynamical downscaling of the western North Pacific from CCSM4 simulations

J. Yoo and J. Galewsky

Table 1. Boundary conditions, forcing that are related with atmospheric concentration ratios of trace gases and Earth's orbital parameters that are applied for the simulations of the modern and the LGM as recommended by the PMIP2 project.

	Ice Sheets	Topography Coastlines	CO_2 (ppmv)	CH_4 (ppbv)	NO_2 (ppbv)	Eccentricity	Obliquity (°)	Angular presession (°)
Modern (0 ka)	Modern	Modern	280	760	270	0.0167724	23.446	102.04
LGM (21 ka)	ICE-5G	ICE-5G	185	350	200	0.018994	22.949	114.42

CPD
doi:10.5194/cp-2015-170

Table 2. CLIMAP LGM vegetation remapped to USGS 24-category land use categories for the LULC over the exposed land surface during the LGM.

	CLIMAP LGM Vegetation	Remapped Cat.		USGS 24-Category
1	Tropical rainforest	13	1	Urban and Built-up Land
2	Monsoon or dry forest	11	2	Dryland Cropland and Pasture
3	Tropical woodland	11	3	Irrigated Cropland and Pasture
4	Tropical thorn scrub and scrub woodland	9	4	Mixed Dryland/Irrigated Cropland and Pasture
5	Tropical semi-desert	9	5	Cropland/Grassland Mosaic
6	Tropical grassland	7	6	Cropland/Woodland Mosaic
7	Tropical extreme desert	19	7	Grassland
8	Savanna	10	8	Shrubland
9	Broadleaved temperate evergreen forest	13	9	Mixed Shrubland/Grassland
10	Montane tropical forest	14	10	Savanna
11	Open boreal woodlands	14	11	Deciduous Broadleaf Forest
12	Semi-arid temperate woodland or scrub	15	12	Deciduous Needleleaf Forest
13	Tundra	22	13	Evergreen Broadleaf
14	Steppe-tundra	20	14	Evergreen Needleleaf
15	Polar and alpine desert	23	15	Mixed Forest
16	Temperate desert	19	16	Water Bodies
17	Temperate semi-desert	9	17	Herbaceous Wetland
18	Forest steppe	17	18	Wooden Wetland
19	Montane Mosaic	15	19	Barren or Sparsely Vegetated
20	Alpine toundra	20	20	Herbaceous Tundra
21	Subalpine parkland	21	21	Wooded Tundra
22	Dry steppe	7	22	Mixed Tundra
23	Temperate steppe grassland	7	23	Bare Ground Tundra
24	Main Taiga	14	24	Snow or Ice
25	Lakes and open water	16		
26	Ice sheet and other permanent ice	24		

CPD
doi:10.5194/cp-2015-170

Table 3. CCSM4 and WRF Model Comparison. The results from the WRF simulations were compared with the CCSM4 LGM paleoclimate and twentieth century simulation results using the ESMF regrid software for the quantitative comparison. 10 year averages of the forecast error (the difference between the WRF and CCSM4 simulations), RMSE, and Normalized forecast error (FE) are shown for evaluated variable ($T2$, SMOIS, TSLB, RH2, $U10$, $V10$, SLP, GHT, TT, UU, and VV. Normalized FE was obtained from (100 × FE/WRF).

VAR	Unit	CCSM4	WRF	Forecast Error	RMSE	Normalized FE
				Modern		
$T2$	C	22.028	19.983	−1.258	3.099	−6.295
SMOIS	$\mathrm{g\,kg^{-1}}$	269.457	254.879	−37.197	104.464	−14.594
TSLB	K	289.007	282.774	−3.053	4.697	−1.079
RH2	%	75.988	84.463	8.7	14.65	10.300
$U10$	$\mathrm{m\,s^{-1}}$	−0.222	−1.996	2.105	5.758	−105.460
$V10$	$\mathrm{m\,s^{-1}}$	−0.027	−0.128	−0.104	4.599	81.261
SLP	hPa	1012.6	1012.72	−0.168	3.807	−0.016
GHT	m	1507.17	1494.86	20.940	103.659	1.400
RH	%	71.710	65.922	6.474	22.186	9.821
TT	K	286.714	286.525	−1.409	19.157	−0.491
UU	$\mathrm{m\,s^{-1}}$	−0.406	−1.387	1.443	6.343	−104.044
VV	$\mathrm{m\,s^{-1}}$	0.216	0.450	0.253	5.281	56.293
				LGM		
$T2$	C	17.035	15.622	−0.466	2.176	−2.986
SMOIS	$\mathrm{g\,kg^{-1}}$	262.023	245.744	−26.558	89.877	−10.807
TSLB	K	286.873	280.315	−3.935	5.350	−1.403
RH2	%	78	82.397	4.628	12.641	5.616
$U10$	$\mathrm{m\,s^{-1}}$	−0.213	−1.756	−1.87	5.561	106.450
$V10$	$\mathrm{m\,s^{-1}}$	−0.020	−0.285	−0.272	4.368	95.466
SLP	hPa	1024.16	1023.75	−0.702	3.482	−0.068
GHT	m	1578.81	1563.51	23.417	109.301	1.497
RH	%	69.724	62.967	−6.942	23.398	−11.026
TT	K	282.304	282.192	−1.391	18.817	−0.493
UU	$\mathrm{m\,s^{-1}}$	−0.177	−0.691	−0.987	5.902	142.825
VV	$\mathrm{m\,s^{-1}}$	0.307	0.231	−0.076	4.924	−32.897

CPD
doi:10.5194/cp-2015-170

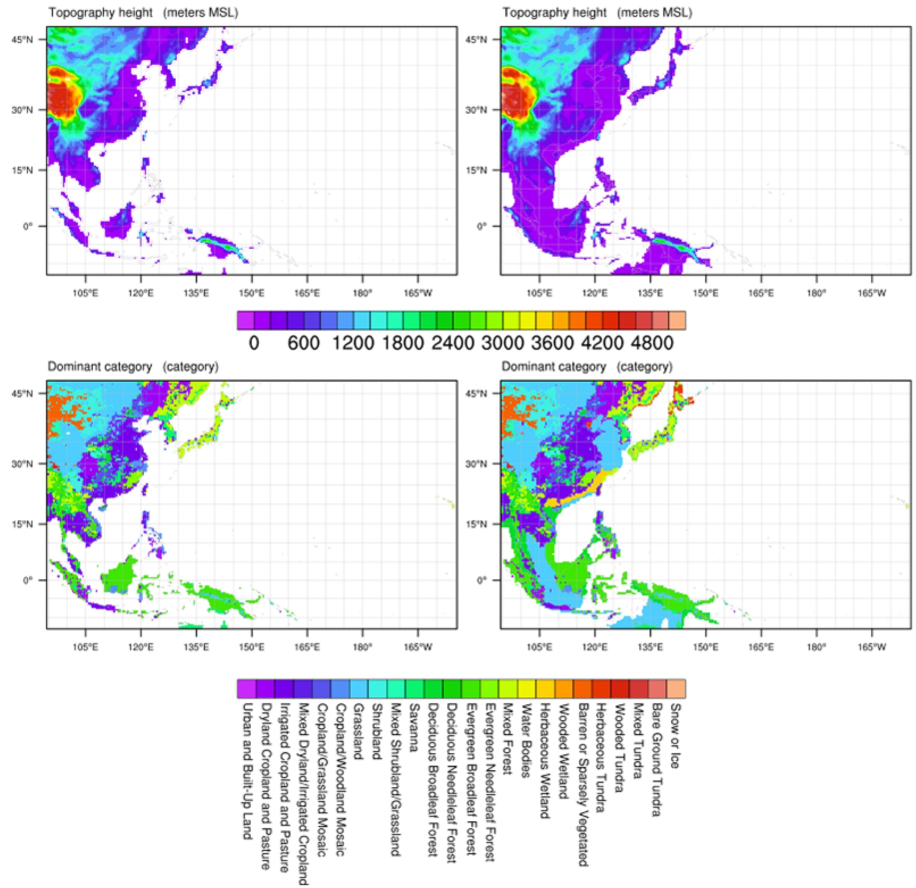

Figure 1. WRF model domains with topography for the Modern (upper left) and LGM (upper right) periods and land use land cover category plots for the Modern (bottom left) and LGM (bottom right) periods. The LGM LULC was reclassified from CLIMAP LGM vegetation into the USGS 24-Category. See Table 1 for the vegetation categories for detail.

CPD

doi:10.5194/cp-2015-170

Dynamical downscaling of the western North Pacific from CCSM4 simulations

J. Yoo and J. Galewsky

Title Page
Abstract | Introduction
Conclusions | References
Tables | Figures
◀I | ▶I
◀ | ▶
Back | Close
Full Screen / Esc
Printer-friendly Version
Interactive Discussion

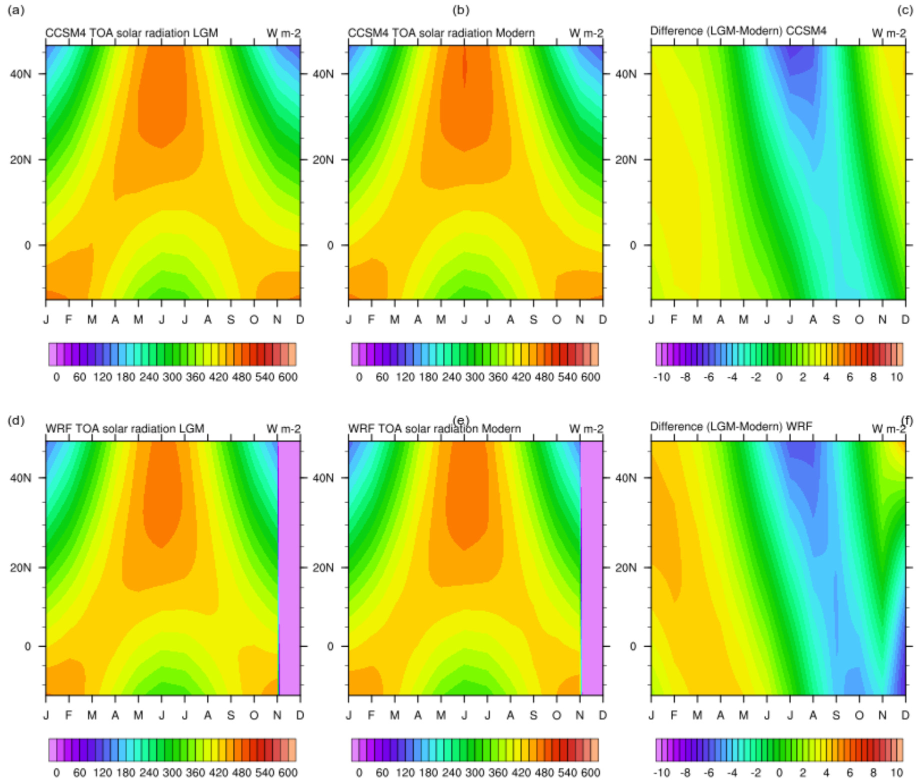

Figure 2. Latitudinal and temporal distribution of incoming solar radiation at the top of atmosphere in the CCSM4 (top) and the WRF model (bottom) simulation for the western North Pacific model domain. **(a)** CCSM4 LGM, **(b)** CCSM4 Modern, **(c)** difference between LGM and Modern in the CCSM4 simulation, **(a)** WRF LGM, **(b)** WRF Modern, and **(c)** difference between LGM and Modern in the WRF simulation.

CPD
doi:10.5194/cp-2015-170

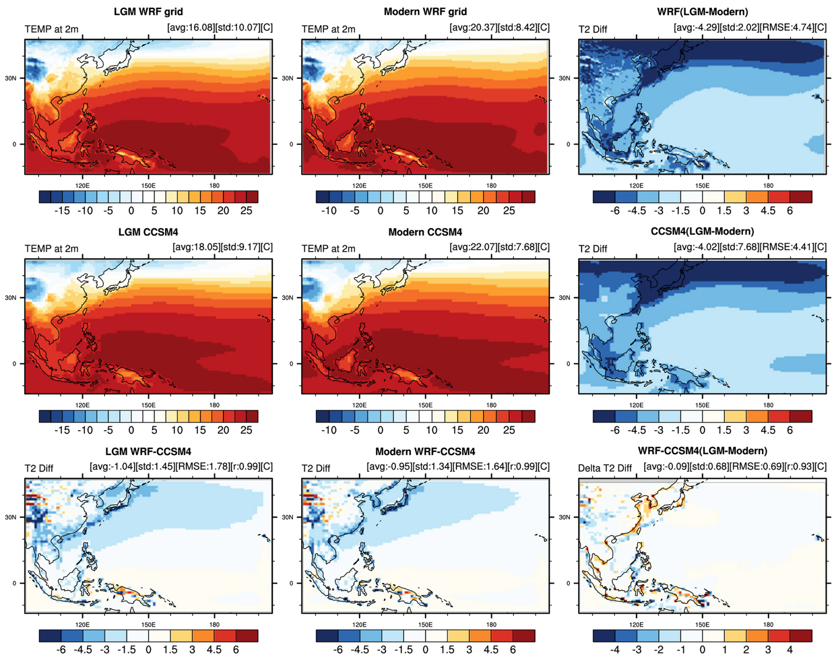

Figure 3. Comparison of ten year averages of 2 m air temperature from WRF and CCSM4 simulations for LGM and late modern periods. Panels on left (center) column show the comparison between the WRF and CCSM4 during the LGM (late modern) period. Bottom plots represent the WRF model biases from CCSM4 results for the LGM, late modern simulation, and their differentials. Top two plots on the right column show the 2 m air temperature differences between the LGM and late modern simulation periods from the WRF (top) and CCSM4 (bottom) simulations. The panel in the lower-right corner shows the difference between the two plots above in the same column. Domain averages and standard deviations are represented at the top of each panel. RMSE is included for the $T2$ difference plots while correlation coefficient is added in the bottom panels.

CPD

doi:10.5194/cp-2015-170

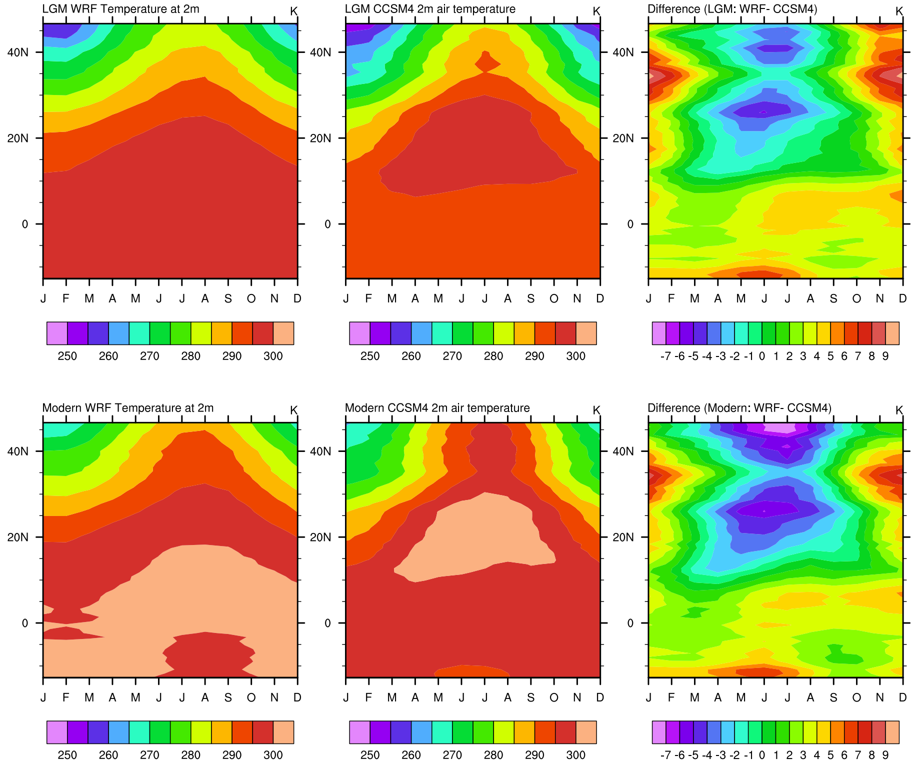

Figure 4. 10 year averages of the latitudinal and monthly distributions of 2 m air temperature ($T2$) from the WRF and CCSM4 simulations and their differences in both the LGM (top) and the Modern (bottom).

CPD
doi:10.5194/cp-2015-170

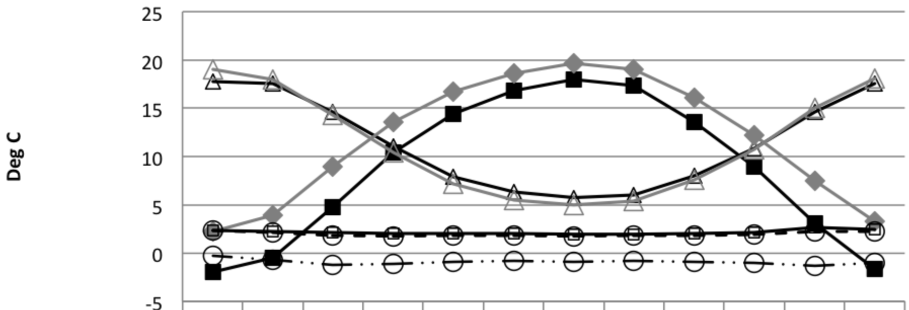

	Jan	Feb	Mar	Apr	May	Jun	Jul	Aug	Sep	Oct	Nov	Dec
WRF T2	-1.99	-0.45	4.81	10.44	14.44	16.81	17.97	17.32	13.62	8.93	3.14	-1.6
WRF Std	17.78	17.55	14.66	11.07	7.88	6.34	5.76	5.98	8	10.88	14.66	17.6
CCSM4 T2	2.23	3.94	8.99	13.58	16.72	18.58	19.62	19.04	16.06	12.17	7.49	3.29
CCSM4 Std	18.98	18.01	14.32	10.47	7.21	5.52	5.01	5.36	7.61	10.76	15.04	18.04
Bias	-0.29	-0.68	-1.23	-1.05	-0.88	-0.8	-0.87	-0.8	-0.88	-1	-1.3	-1.03
Bias Std	2.39	2.12	1.82	1.78	1.86	1.85	1.78	1.8	1.85	1.95	2.29	2.26
RMSE	2.4	2.23	2.2	2.06	2.06	2.02	1.98	1.97	2.05	2.2	2.64	2.48

Figure 5. 10 year monthly climate of 2 m air temperature ($T2$) and standard deviation (SD) from the WRF and CCSM4 simulations and the WRF model bias in the LGM.

CPD
doi:10.5194/cp-2015-170

J. Yoo and J. Galewsky

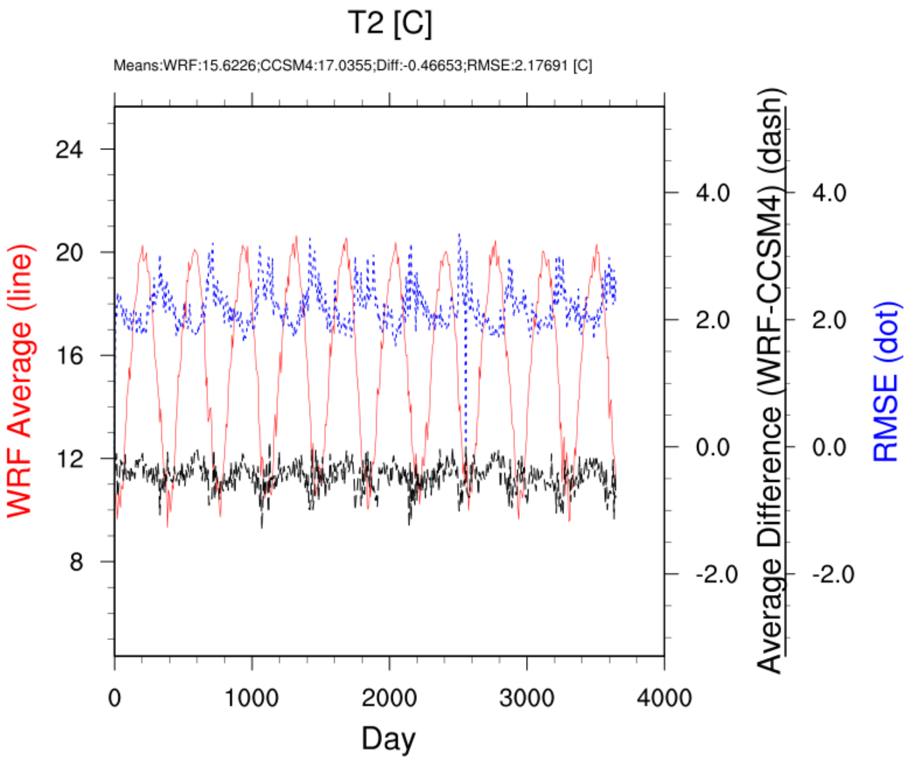

Figure 6. Time series of 2 m air temperature for ten years in the WRF and CCSM4 simulations for the LGM period. Domain averages of the WRF model result, their forecast error (WRF-CCSM4), and the RMSE between the WRF and CCSM4 are plotted with red (line), black (dash line), and blue (dot line), respectively.

CPD
doi:10.5194/cp-2015-170

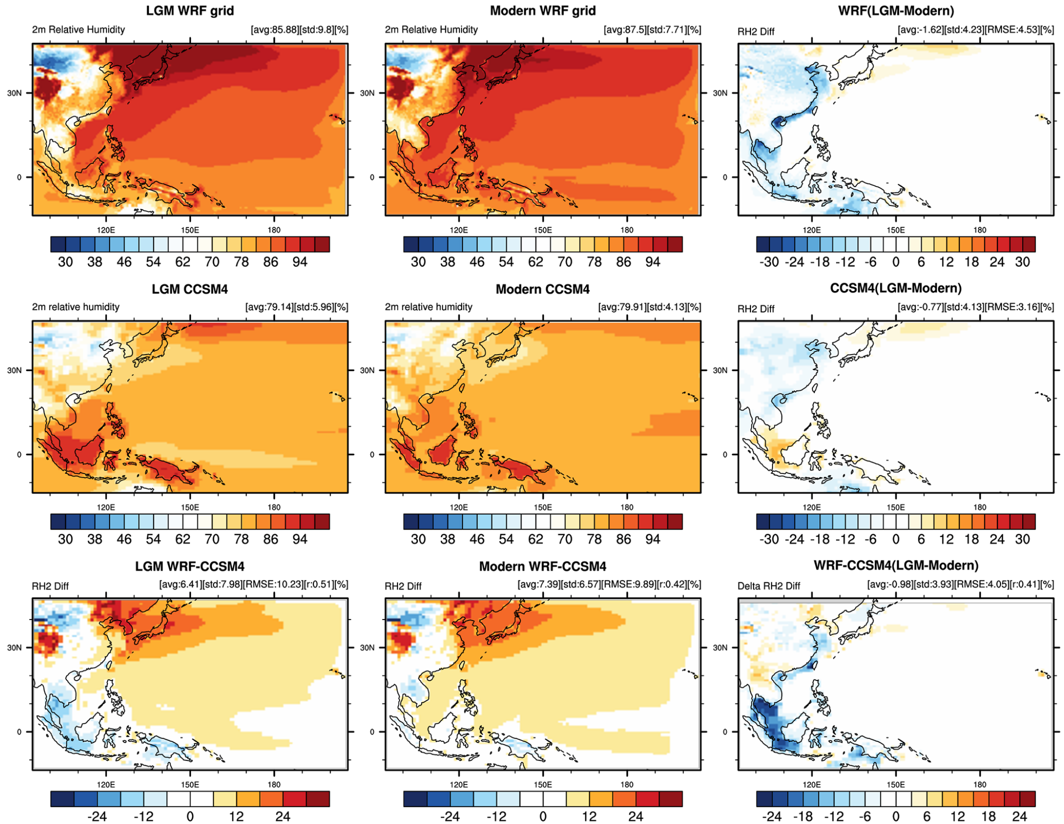

Figure 7. As in Fig. 3 but for 2 m relative humidity.

CPD
doi:10.5194/cp-2015-170

Dynamical downscaling of the western North Pacific from CCSM4 simulations

J. Yoo and J. Galewsky

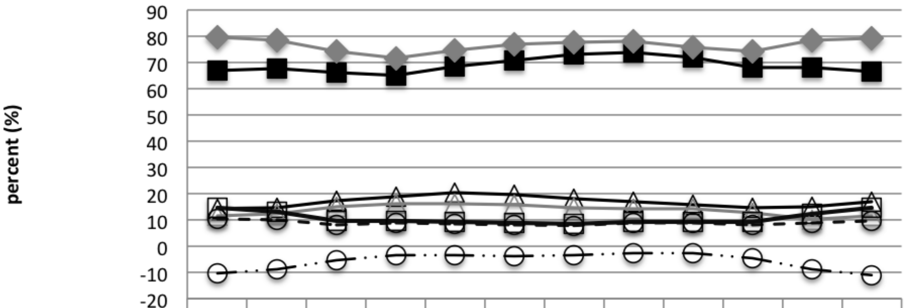

	Jan	Feb	Mar	Apr	May	Jun	Jul	Aug	Sep	Oct	Nov	Dec
WRF RH2	66.92	67.92	66.14	65.11	68.38	70.81	73.01	74.02	71.96	67.99	68.09	66.65
WRF Std	14.39	14.73	17.18	18.83	20.36	19.76	17.99	16.86	15.79	14.6	15.02	16.93
CCSM4 RH2	79.82	78.68	74.08	71.73	74.74	76.86	77.92	77.96	75.98	74.13	78.35	79.28
CCSM4 Std	11.71	12.43	14.99	16.2	16.17	15.74	14.54	14.3	14.12	12.87	10.25	11.59
Bias	-10.28	-8.59	-5.46	-3.57	-3.46	-3.74	-3.25	-2.7	-2.66	-4.37	-8.62	-11.01
Bias Std	10.29	9.94	8.21	8.98	8.61	8.03	7.89	8.73	8.76	8.1	9	9.74
RMSE	14.55	13.13	9.86	9.66	9.28	8.86	8.54	9.14	9.16	9.2	12.46	14.7

Figure 8. As in Fig. 5 but for 2 m relative humidity (RH2).

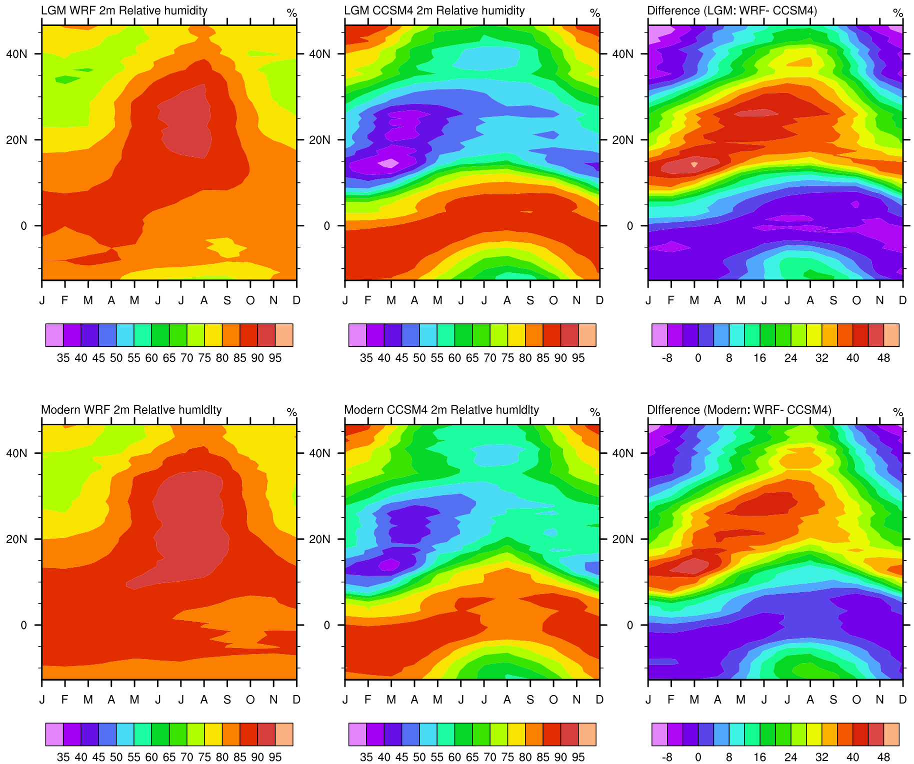

Figure 9. As in Fig. 4 but for 2 m relative humidity (RH2).

CPD
doi:10.5194/cp-2015-170

Dynamical downscaling of the western North Pacific from CCSM4 simulations

J. Yoo and J. Galewsky

Title Page
Abstract Introduction
Conclusions References
Tables Figures
◀◀ ▶▶
◀ ▶
Back Close
Full Screen / Esc
Printer-friendly Version
Interactive Discussion

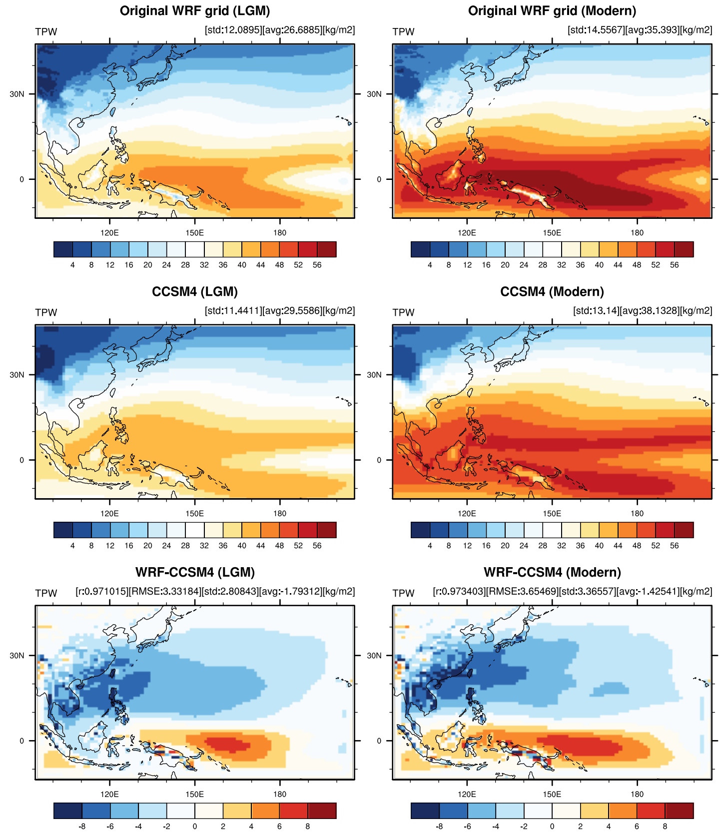

Figure 10. 10 year averages of total precipitable water (TPW) in LGM (left column) and modern (right column) from the WRF (top) and CCSM4 (middle) simulations and the WRF model bias (bottom). Domain averages and standard deviations are represented at the top of each panel. Correlation coefficient (*r*) and RMSE are included for the model bias plots (bottom).

CPD
doi:10.5194/cp-2015-170

Dynamical downscaling of the western North Pacific from CCSM4 simulations

J. Yoo and J. Galewsky

Title Page
Abstract | Introduction
Conclusions | References
Tables | Figures
Back | Close
Full Screen / Esc
Printer-friendly Version
Interactive Discussion

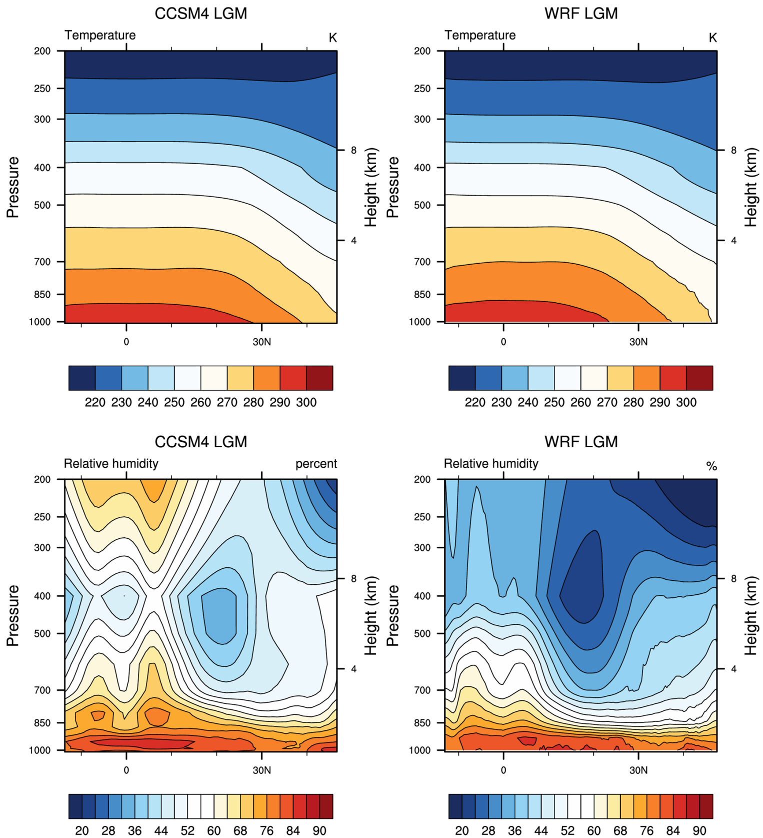

Figure 11. Vertical and latitudinal plots of the ten years zonal averages of atmospheric temperature (T; top) and relative humidity (RH; bottom) comparing CCSM4 (left) and WRF (right) results from their LGM simulations.

CPD
doi:10.5194/cp-2015-170

Dynamical downscaling of the western North Pacific from CCSM4 simulations

J. Yoo and J. Galewsky

Title Page
Abstract Introduction
Conclusions References
Tables Figures
◀ ▶
Back Close
Full Screen / Esc
Printer-friendly Version
Interactive Discussion

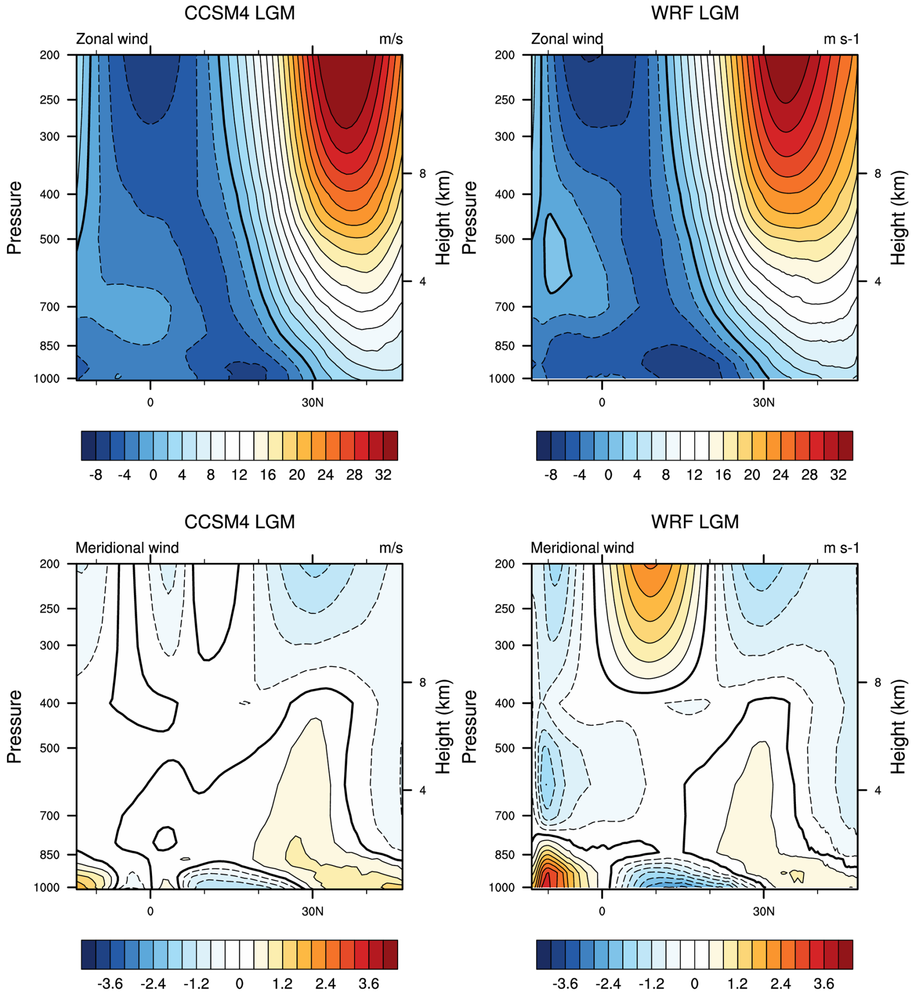

Figure 12. As in Fig. 11 but for zonal wind (U; top) and meridional wind (V; bottom).

CPD
doi:10.5194/cp-2015-170

Dynamical downscaling of the western North Pacific from CCSM4 simulations

J. Yoo and J. Galewsky